Diafiltration by Nanofiltration: Prediction and Optimization

W. Richard Bowen and A. Wahab Mohammad
Biochemical Engineering Group, Centre for Complex Fluids Processing, Dept. of Chemical and Biological Process Engineering, University of Wales Swansea, Swansea SA2 8PP, U.K.

A predictive model for the performance of a nanofiltration membrane in separating the components of a dye/salt solution was developed. It is based on the extended Nernst-Planck equation with incorporation of concentration polarization for mixtures of charged ions. Excellent agreement between predicted and experimental rejections of anions and cations was obtained for batch nanofiltration at different ratios of dye/salt assuming that the membrane charge density (X_d) depends on the total concentration of negative charges in the solutions. Prediction for diafiltration experiments was also excellent by allowing for variation in X_d as the salt concentration in the solution changed as a function of time. The model was used to investigate optimization of the processing conditions. The overall diafiltration process operated best in a two-phase mode, in which the dye solution was preconcentrated to the final required dye concentration before diafiltration.

Introduction

Nanofiltration (NF) membranes are a new class of membrane which have properties in between those of ultrafiltration (UF) membranes and reverse-osmosis (RO) membranes. Their separation mechanisms involve both steric (sieving) effects and electrical (Donnan) effects. This combination allows NF membranes to be effective for a range of separations of mixtures of small organic solutes (either neutral or charged) and salts (Raman et al., 1994).

The ability to predict the process performance of NF membrane separations would be very useful for the planning and optimization of processes. Such predictions would ideally utilize available physical property data of a process stream and a membrane. For NF membranes, this would involve the structural parameters such as the pore radius and membrane thickness, and the electrical parameters, such as the surface charge density or the volumetric charge density. In this article, an example of such a prediction will be presented for the diafiltration of dye/salt solutions using an NF membrane. Diafiltration of dye solutions is an industrially important process. NF membranes are especially suited for such processes since, through the combination of steric and Donnan effects, the dye will be highly rejected while the salts may even be negatively rejected (concentrated in the permeate).

Two main approaches have been used thus far to model the transport of ionic species through NF membranes. One approach is through the Spiegler-Kedem model (Spiegler and Kedem, 1966; Jitsuhara and Kimura, 1983; Perry and Linder, 1989; Schirg and Widmer, 1992; Levenstein et al., 1996). This black-box approach allows the membranes to be characterized in terms of salt permeability P_s and the reflection coefficient σ. This model is in the first instance limited to binary salt systems, and in the limiting case to a binary salt system in the presence of a completely rejected organic ion (Perry and Linder, 1989; Schirg and Widmer, 1992).

The second approach is based on the extended Nernst-Planck equation. Through this approach, a system containing any number of n ions can be described using a set of $(3n+2)$ equations. Tsuru et al. (1991a) first proposed such a model for NF membranes, describing the transport of ions in terms of an effective membrane thickness/porosity ratio (m) $\Delta x/A_k$ and an effective membrane charge density (mol·m^{-3}) X_d. The model was successful in describing the rejection of mixed salt solutions (Tsuru et al., 1991b). In later work (Wang et al., 1995a,b), a similar model but with the inclusion of steric effects was used to model the transport of an organic electrolyte in the presence of Na^+ and Cl^- ions. In a recent

Correspondence concerning this article should be addressed to W. R. Bowen.

work, Rios et al. (1996) proposed a simpler model whereby the diffusion term in the Nernst-Planck equation was assumed to be negligible.

Bowen and Mukhtar (1996) proposed a hybrid model (HM) based on the extended Nernst-Planck equation to describe the transport of salts in binary and ternary systems. The model was solved as if the membrane were homogenous and nonporous, but hindrance effects for diffusion and convection were included to allow for the transport of ions taking place within a confined space inside the membranes. This inclusion allows the membrane to be characterized in terms of an effective pore radius r_p in addition to $\Delta x/A_k$ and X_d. The model was successful in predicting the separation performance of a ternary salt system (Na^+: Cl^-: SO_4^{2-}). The negative rejection of Cl^- at low flux was explained in terms of the interplay between diffusion, convection, and electromigration mechanisms. In a recent article, Bowen et al. (1997) used atomic force microscopy (AFM) to show the presence of well-formed pores in an NF membrane. Thus, it is more appropriate to describe the transport of ions as occurring through discrete pores rather than using a homogenous description of the membrane structure. Such a description was termed a Donnan-steric pore model (DSPM) (Bowen et al., 1997). Membranes may then be characterized in terms of r_p, $\Delta x/A_k$, and X_d using the rejection data of uncharged solutes and salts. It was concluded that r_p and $\Delta x/A_k$ were most easily determined using rejection data for uncharged solutes, while rejection data of binary salts allowed determination of X_d in addition to these parameters.

There have not been many published works on the modeling of the separation performance of solutions containing dyes and salts in nanofiltration membrane systems. Perry and Linder (1989) reported the use of NF membranes (referred to in their article as intermediate reverse osmosis ultrafiltration membranes) for solutions containing charged organics and NaCl. They observed that increase in concentration of the retained charged organics caused the salt rejection to become even more negative. The negative rejection of the salt thus provided an opportunity to have a very effective desalination without excessive diafiltration. Even if diafiltration is still needed, the required washing volume will be reduced in proportion to the negative values of the salt rejection. However, no experiments or modeling of a diafiltration process were carried out.

Similar results have been observed by different groups (Schirg and Widmer, 1992; Levenstein et al., 1996). Levenstein et al. (1996) reported the use of a large polyelectrolyte (60000 D) in a dye-salt system to further enhance the removal of NaCl from the solutions. In all of these works, the rejection model used was based on the Spiegler-Kedem approach. Levenstein et al. (1996) modified the model by neglecting the convective term in the Spiegler-Kedem equation. The effects of concentration polarization were taken into account only for a binary salt system, not for a system with a mixture of ions.

The main objective of the present study was to model the process of diafiltration of a dye solution containing salt (NaCl). The factors controlling such a process are extremely complex, and the challenge is to find a theoretical description which, despite some approximations, can give good predictions for engineering purposes. The membrane was first characterized in terms of the effective pore radius (r_p), the effective ratio of membrane thickness over porosity ($\Delta x/A_k$), and the volumetric charge density (X_d) obtained using the rejection data of uncharged solutes and salts in combination with a Donnan-steric pore model (Bowen et al., 1997). Using the three parameters obtained, prediction of the separation performance of dye/salt solutions was made and compared to experimental data. A description of the solution concentration polarization for mixtures of charged solutes was also included in the model. The use of such a model not only allows one to optimize the diafiltration process but also to select the membrane with optimum properties.

Theoretical Background

Transport equations inside the membranes

The extended Nernst-Planck equation forms the basis for the description of the transport of ions/solutes inside porous membranes. The equation can be written as

$$j_i = -D_{i,p}\frac{dc_i}{dx} - \frac{z_i c_i D_{i,p}}{RT}F\frac{d\psi_m}{dx} + K_{i,c}c_i V \qquad (1)$$

where

$$D_{i,p} = K_{i,d}D_{i,\infty} \qquad (2)$$

j_i is the flux of ion i and the terms on the righthand side represent transport due to diffusion, electric field gradient, and convection, respectively. The effect of pressure on the chemical potential (and hence diffusion) is not included in Eq. 1 as this may be calculated to be negligible for the operating conditions ($\Delta P \leq 500$ kPa) and solutes being transported across the membrane in the present work (Dickson, 1988; Burghoff et al., 1980). Equation 1 also does not take into account the effect on $D_{i,p}$ of specific ion membrane matrix interactions. A Maxwell-Stefan approach could take such interactions into account, but is impossible to apply due to lack of data. Furthermore, the Nernst-Planck equation has been shown to give excellent agreement with experimental data for diffusion in a charged porous matrix, even for the extreme case of ion-exchange (Helfferich, 1983; Krishna and Wesselingh, 1997).

The hindered nature of diffusion and convection of the ions inside the membrane are accounted for by the terms $K_{i,d}$ and $K_{i,c}$. The hindrance factors $K_{i,d}$ and $K_{i,c}$, which are functions of the ratio of solute to pore radius (λ), are related to the hydrodynamic coefficients K^{-1} (the enhanced drag) and G (the lag coefficient of a spherical solute moving inside a cylindrical pore of infinite length). Deen (1987) reviewed the various equations that have been used to calculate K^{-1} and G for centerline approximations. Recent work (Bowen and Sharif, 1994) uses the finite-element technique and a centerline approach to calculate values of K^{-1} and G for λ ranging from 0 to 0.95. These values will be used in the present work.

Thus, for $0 < \lambda < 0.95$, the enhanced drag and the lag coefficients have been calculated using

$$K^{-1}(\lambda,0) = 1.0 - 2.30\lambda + 1.154\lambda^2 + 0.224\lambda^3 \qquad (3)$$

$$G(\lambda,0) = 1.0 + 0.054\lambda - 0.988\lambda^2 + 0.441\lambda^3 \qquad (4)$$

The solute velocity is assumed to be fully developed inside the pore with a parabolic profile of the Hagen-Poiseuille type. The hindrance factors are then expressed as (Deen, 1987),

$$K_{i,d} = K^{-1}(\lambda,0) \qquad K_{i,c} = (2-\Phi)G(\lambda,0) \tag{5}$$

where

$$\Phi = (1-\lambda)^2 \tag{6}$$

The steric term Φ accounts for the finite size of the solute. In solving the basic equation for the transport of ions inside the membrane (Eq. 1), the fluxes, concentrations, potentials, and velocity were all defined in terms of radially averaged quantities. The conditions of electroneutrality in the bulk solution and inside the membranes are expressed, respectively, as,

$$\sum_{i=1}^{n} z_i C_i = 0 \qquad \sum_{i=1}^{n} z_i c_i = -X_d \tag{7}$$

where C_i is the bulk concentration of ion i (mol·$\overline{\text{m}}^3$), c_i is the concentration of ion i inside the membrane (mol·$\overline{\text{m}}^3$), and X_d is the effective volumetric membrane charge density (mol·$\overline{\text{m}}^3$). X_d is assumed to be constant at all points in the active part of the membrane. The zero current condition inside the membrane is expressed as

$$I_c = \sum_{i=1}^{n} F(z_i j_i) = 0 \tag{8}$$

Since the electric potential gradient is common for every ion inside the membrane, then the electric potential and concentration gradients can be derived from Eq. 1. By rearranging Eq. 1, the concentration gradient is written as

$$\frac{dc_i}{dx} = \frac{J_v}{D_{i,p}}(K_{i,c}c_i - C_{i,p}) - \frac{z_i c_i}{RT}F\frac{d\psi_m}{dx} \tag{9}$$

where the flux of ion j_i (mol·m^{-2}·s^{-1}) is expressed as

$$j_i = J_v C_{i,p} \tag{10}$$

Similarly, the potential gradient term can be expressed as

$$\frac{d\psi_m}{dx} = \frac{\sum_{i=1}^{n} \frac{z_i J_v}{D_{i,p}}(K_{i,c}c_i - C_{i,p})}{\frac{F}{RT}\sum_{i=1}^{n}(z_i^2 c_i)} \tag{11}$$

Equations 9 and 11 can be solved by using the following boundary conditions together with the equation for electroneutrality (Eq. 7)

$$\text{at} \qquad x = 0 \quad C_i = C_{i,w}; \qquad x = \Delta x \quad C_i = C_{i,p} \tag{12}$$

where $C_{i,w}$ and $C_{i,p}$ are the feed and permeate concentrations of ion i at the interfaces of the membrane (mol·m^{-3}), respectively. These are the concentrations just outside the membrane. The concentration at the interface (that is, just inside the membrane) can be determined using the following equilibrium conditions which will be taken as a combination of the Donnan and steric effects (Deen et al., 1980)

$$\left(\frac{\gamma_i c_i}{\gamma_i^0 C_i}\right) = \Phi \exp\left(-\frac{z_i F}{RT}\Delta\psi_D\right) \tag{13}$$

The term Φ is the steric partitioning term to account for the steric effects on entrance to the membrane and is given by Eq. 6. We have previously shown, through solution of the nonlinear Poisson-Boltzmann equation, that the assumption of a Donnan type of partitioning is well justified for conditions such as those in the present work, as the variation in potential across the membrane pores is very small (Bowen et al., 1997). This is likely to be the case for most true nanofiltration membranes (as opposed to ultrafiltration membranes) under most practical operating conditions. In the application of Eq. 13 it is assumed that $\gamma_i^0 = 1$ and $\gamma_i = 1$, as the salt concentrations in solution are relatively low, and it is very difficult to obtain information about the activity coefficients in the membrane. However, the procedures used in the present work take some implicit account of activity coefficients as experimental data is used to derive an isotherm relating membrane charge density to solution concentrations (Eq. 38 and Figure 8).

For transport of uncharged solutes across the membrane, there will be no electrostatic term in Eq. 1. The rejection can be expressed as

$$R_{\text{real}} = 1 - \frac{C_{i,p}}{C_{i,w}} = 1 - \frac{K_{i,c}\Phi}{1-\exp(-Pe_m)[1-\Phi K_{i,c}]} \tag{14}$$

where the Peclet number Pe_m is defined as

$$Pe_m = \frac{K_{i,c}}{K_{i,d}}\frac{V\Delta x}{D_{i,\infty}A_k} \tag{15}$$

In the limiting case of the $Pe_m \to \infty$, the asymptotic rejection values will approach $(1-\Phi K_{i,c})$. Thus, $(1-\Phi K_{i,c})$ represents a parameter for comparing the limiting rejections of solutes of various sizes.

The Hagen-Poiseuille equation gives the relationship between the pure water flux and the applied pressure across the membrane (Nakao and Kimura, 1981)

$$J_w = \frac{r_p^2 \Delta P}{8\mu(\Delta x/A_k)} \tag{16}$$

Description of concentration polarization

Figure 1 shows the interface between the bulk solution and the membrane surface for a three component system. Concentration polarization close to the membrane surface is assumed to occur within a boundary film layer of thickness δ

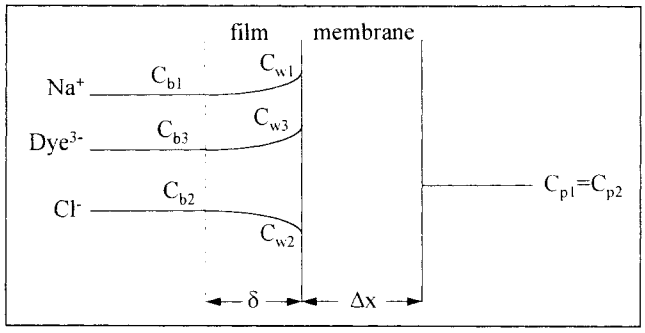

Figure 1. Film layer and membrane for three-component system.

(m). For a system containing charged ions, a mass balance for the film layer yields

$$j_i = -D_{i,\infty}\frac{dC_i}{dx} - \frac{z_i F}{RT}C_i D_{i,\infty}\frac{d\psi_f}{dx} + C_i J_v \tag{17}$$

This is similar to Eq. 1 except that now the diffusivity is the bulk diffusivity in the solution. The net solute flux is defined as in Eq. 10. The equation can be solved using the boundary conditions: at $x = -\delta$, $c = C_{i,b}$ and at $x = 0$, $c = C_{i,w}$.

For a binary salt, the cation and anion will move together due to the requirement of electroneutrality. Equation 17 can be solved for both ions and the flux expressed as

$$j_+ = j_- = -D_{\text{eff},\infty}\frac{dC_\pm}{dx} + C_\pm J_v \tag{18}$$

where $D_{\text{eff},\infty}$ is the effective diffusivity of the salt ($m^2 \cdot s^{-1}$) defined as (Krishna and Wesselingh, 1997)

$$D_{\text{eff},\infty} = \frac{D_+ D_- (z_+ - z_-)}{z_+ D_+ - z_- D_-} \tag{19}$$

Using the boundary condition defined above, the wall concentration C_w can be correlated to other measurable parameters as

$$\frac{J_v}{k} = \ln\frac{(C_w - C_p)}{(C_b - C_p)} \tag{20}$$

This result is also applicable to uncharged solute systems. Here k is the mass-transfer coefficient ($m \cdot s^{-1}$) in the polarized boundary layer and for a charged binary system is defined as

$$k = \frac{D_{\text{eff},\infty}}{\delta} \tag{21}$$

The mass-transfer coefficient is often characterized by a Sherwood number (N_{Sh}) correlation which is expressed as a function of Reynolds number (N_{Re}) and Schmidt number (N_{Sc}). For a stirred cell, the correlation is given as (Smith et al., 1968; Opong and Zydney, 1991)

$$N_{Sh} = \frac{kr}{D_{\text{eff},\infty}} = \varphi(N_{Re})^n (N_{Sc})^{0.33} \tag{22}$$

where

$$N_{Re} = \frac{\omega r^2}{\upsilon}, \qquad N_{Sc} = \frac{u}{D_{\text{eff},\infty}} \tag{23}$$

We have shown (Bowen et al., 1997), by using the infinite rejection method proposed by Nakao and Kimura (1981), that for our experimental setup, the mass-transfer coefficient can be expressed as

$$k = 0.23\left(\frac{r^2}{\upsilon}\right)^{0.567}\left(\frac{\upsilon}{D_{\text{eff},\infty}}\right)^{0.33}\frac{D_{\text{eff},\infty}}{r}\omega^{0.567} \tag{24}$$

For solutions containing more than two charged ions/solutes, it is difficult to obtain analytical solutions to Eq. 17. The equations can, however, be solved numerically. In this work, the solutions for the transport in the film layer will be solved together with the transport equations inside the membrane. The boundary condition at the wall ($C_{i,w}$) is coupled with the Donnan-steric equilibrium conditions (Eq. 13). The solution in the film layer, however, requires one parameter δ which will be determined from the individual mass-transfer coefficients of the ions from Eq. 21 and Eq. 24. The values of k, however, vary with diffusivities, and, consequently, δ varies as well. It will be assumed in the present work that since the dye has the lowest diffusivity, the transport will be controlled by the movement of the dye. Thus, δ will be taken as that obtained from the dye mass-transfer coefficient using the diffusion coefficient of the dye.

Wesselingh and Vonk (1995) proposed similar equations for describing the polarization behavior of a polyelectrolyte with small ions in an ultrafiltration membrane system. Their approach was based on the generalized Maxwell-Stefan equations which take into account the frictional interactions between all species. For solutions of low concentrations, the interactions between solutes can be ignored (Krishna and Wesselingh, 1997) and only the interaction between each solute and the solvent is taken into account. Such is the case that will be described in the present work.

Description of diafiltration process

The overall process of diafiltration may involve the pre- and post-concentration of the solutions (Dutre and Tragardh, 1994). In the first instance in the present work, only the actual diafiltration step will be simulated and compared to the experimental data obtained. The diafiltration process will be a batch-continuous process at constant applied pressure and constant volume of the feed solution. Subsequently, the model will be used to optimize the normalized time for the overall process which includes pre- and post-concentration phases.

Diafiltration Phase. If C_{sf} is the bulk concentration of salt in the feed and C_{sp} is the bulk concentration of salt in permeate, a mass balance on salt in the system gives

$$\frac{d(V_f C_{sf})}{dt} = -J_v A C_{sp} \tag{25}$$

thus

$$C_{sf}\frac{dV_f}{dt}+V_f\frac{dC_{sf}}{dt}=-J_vAC_{sp} \tag{26}$$

Since the volume is constant, Eq. 26 can be written as

$$\int_{t_{d0}}^{t_{d1}}dt=t_{d1}-t_{d0}=\int_{C_{sf,t_{d0}}}^{C_{sf,t_{d1}}}-\frac{V_f}{J_vA}\frac{1}{C_{sp}}dC_{sf} \tag{27}$$

In order to calculate the time for the diafiltration phase, the righthand side of Eq. 27 needs to be integrated. $C_{sf,t_{d1}}$ is the final concentration of salt in the feed. Equation 27 can be expressed in terms of the observed rejection R_{obs} as follows

$$\int_{t_{d0}}^{t_{d1}}dt=t_{d1}-t_{d0}=-\frac{V_f}{A}\int_{C_{sf,t_{d0}}}^{C_{sf,t_{d1}}}\frac{1}{J_vC_{sf}(1-R_{obs})}dC_{sf} \tag{28}$$

Pre and Post-Concentration Phases. The concentration phase is more complicated since both the dye and salt concentrations change continuously during this phase. A mass balance for the dye gives

$$\frac{d(V_fC_{dye\,f})}{dt}=0 \tag{29}$$

thus

$$C_{dye\,f}\frac{dV_f}{dt}+V_f\frac{dC_{dye\,f}}{dt}=0 \tag{30}$$

Since the dye is expected to be fully retained in the feed, V_f is related to the mass and concentration of the dye as

$$V_f=\frac{M_{dye}}{C_{dye\,f}} \tag{31}$$

The change in V_f is related to the permeate flux and the membrane area as follows

$$\frac{dV_f}{dt}=-AJ_v \tag{32}$$

Substituting Eqs. 31 and 32 into Eq. 30 yields

$$\frac{dC_{dye\,f}}{dt}=\frac{AJ_v}{M_{dye}}C_{dye\,f}^2 \tag{33}$$

thus,

$$\int_{t_{c0}}^{t_{c1}}dt=t_{c1}-t_{c0}=\frac{M_{dye}}{A}\int_{C_{dye\,f,t_{c0}}}^{C_{dye\,f,t_{c1}}}\frac{1}{J_vC_{dye\,f}^2}dC_{dye\,f} \tag{34}$$

Equation 34 can be used to calculate the time for concentrating the dye solution from $C_{dye\,f,t_{c0}}$ to $C_{dye\,f,t_{c1}}$. It depends only on the permeate flux and the dye concentrations. A similar mass balance for the salt yields the following equation

$$\frac{dC_{sf}}{dt}=\frac{AJ_v}{M_{dye}}C_{dye\,f}C_{sf}R_{obs} \tag{35}$$

Dividing Eq. 35 by 33 allows calculation of the change in salt concentration as a function of dye concentration in the solution

$$\frac{dC_{sf}}{dC_{dye\,f}}=\frac{C_{sf}R_{obs}}{C_{dye\,f}} \tag{36}$$

Thus

$$\ln\left(\frac{C_{dye\,f,t_{c1}}}{C_{dye\,f,t_{c0}}}\right)=\int_{C_{sf,t_{c0}}}^{C_{sf,t_{c1}}}\frac{1}{C_{sf}R_{obs}}dC_{sf} \tag{37}$$

Computer algorithm

For a system of n ions, there will be one equation for the potential gradient (Eq. 11) and n equations for the concentration gradient (Eq. 9). For simulation purposes, the following variables are fixed: J_v, $\Delta x/A_k$, r_p, X_d, and $C_{1,b}$, $C_{2,b}$, ..., $C_{n,b}$. The unknown variables would be: $c_1, c_2, \ldots, c_n]_{x=0}$, $c_1, c_2, \ldots, c_n]_{x=\Delta x}$, $C_{1,p}$, $C_{2,p}$, ..., $C_{n,p}$ and $\Delta\psi_{D,0}$, $\Delta\psi_{D,\Delta x}$, ψ_m. Thus, the total unknown variables would be $3n+3$. There will also be n Donnan equations at $x=0$, n Donnan equations at $x=\Delta x$, and one equation for electroneutrality inside the membrane. The total equations then will be $3n+2$. Thus, an iterative method is needed in order to determine the unknown variables. Theoretically, however, it is possible to solve the equations for any given number of ions. A further simplification can be made for binary and ternary salt systems whereby the Donnan equation can be solved and the concentrations of each ion at $x=0$ and $x=\Delta x$ can be determined from polynomial equations in terms of X_d, C_w, and C_p (Rios et al., 1996).

The differential equations for concentration and potential gradients were solved using the Runge-Kutta-Gill method as proposed by Tsuru et al. (1991a). The solutions were combined with the numerical algorithm group (NAG) routine C05NBF, which is a routine to find a zero of a system of nonlinear functions in n variables by modification of the Powell hybrid method. The diafiltration time was integrated numerically using the trapezoidal rule with a large subdivision of the integral limits.

Experimental Work

The NF membrane used in this work was the CA30 membrane obtained from Hoechst Separation Products (Germany). This membrane is a Nadir proprietary cellulose acetate (CA) membrane. The experimental setup was essentially the same as described in previous work (Bowen and Mukhtar, 1996; Bowen et al., 1997). All experiments were carried out at 25°C and pH of 5.8–6.0, which is the pH of the ultrapure water used in preparing all the samples.

Table 1. Properties of Ions and Uncharged Solutes

Ions/Solutes	AW or MW ($g \cdot mol^{-1}$)	D_∞ ($m^2 \cdot s^{-1}) \times 10^{-9}$	r_s (nm)
K^+	39	1.95	0.125
Na^+	23	1.33	0.184
Li^+	7	1.03	0.238
Cl^-	35	2.03	0.121
Glycerin	92	0.95	0.260
Glucose	180	0.69	0.365
Sucrose	342	0.52	0.471
Vitamin B_{12}	1,355	0.33	0.740

AW = atomic weight; MW = molecular weight.

Characterization of membrane

The salts used in the experiments were KCl, NaCl, and LiCl in high purity forms obtained from Fischer Scientific UK. The permeate concentrations of salts were determined from conductivity measurements. The neutral solutes used were vitamin B_{12}, sucrose, glucose, and glycerin. They were also from Fischer Scientific UK. The concentrations of vitamin B_{12} were analyzed using a Spectrophotometer at 361 nm. Concentrations of the other solutes were determined using enzymatic assay kits (Boehringer Mannheim, 1996) obtained from Boehringer Mannheim UK. Table 1 lists the properties of the salts and the neutral solutes. The diffusivity data were obtained from published works (Nakao and Kimura, 1981; Atkins, 1990) except for the dye which was determined experimentally, as will be described later. Effective spherical radii were calculated using the Stokes-Einstein equation. The cation radii reflect their differing degrees of hydration.

Permeation experiments with KCl, NaCl, and LiCl were carried out using a 200 mL stirred Amicon cell (Model 8200) as previously described (Bowen and Mukhtar, 1995). The concentration used was 10^{-2} M, and the stirring speed was 300 rpm, both unless otherwise stated. The applied pressure was in the range 100–500 $kN \cdot m^{-2}$. Similar permeation experiments were carried out with the neutral molecules. The concentration used ranged from 0.1–0.3 $kg \cdot m^{-3}$.

Characterization of the dye

The dye sample provided by Zeneca has a molecular weight of 721.5 in free acid form or 787.5 as sodium salt. Figure 2 shows the chemical structure of the reactive red dye. The sample that was provided was 95% pure. The other 5% consists of an uncharged variation of the dye molecules and other inorganic impurities. The dye sample was not purified further since the original sample is more representative of the real solution occurring in industry.

The dye can be assayed at 535 nm using a spectrophotometer. The extinction coefficient (ϵ) of the dye is 0.0614 $L \cdot mol^{-1} \cdot cm^{-1}$. The diffusion coefficient of the dye was determined from measurement of the electrical conductivity of the dye solutions at different concentrations (see Appendix for theory). Again, the measurements were made at 25°C.

Diafiltration experiments

Two types of nanofiltration experiments were carried out with dye/salt solutions. The first type was carried out to confirm the validity of the transport model. Permeation experiments involving dye solutions at different dye/salt ratios were carried out at constant pressure of 500 $kN \cdot m^{-2}$. The dye concentrations were fixed at 37 $mol \cdot m^{-3}$ and 4 $mol \cdot m^{-3}$, respectively. The salt concentrations in the solutions were varied from 5 to 100 $mol \cdot m^{-3}$. The procedures were similar to those used in the salts and uncharged solutes experiments. In all diafiltration experiments, the stirring speed was set at 400 rpm.

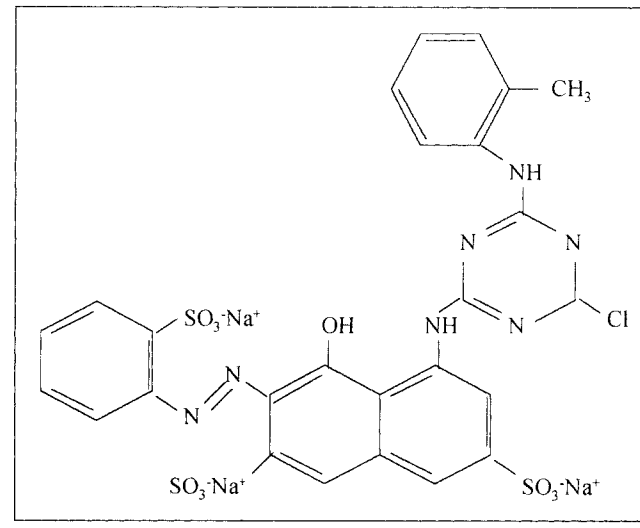

Figure 2. Molecular structure of the reactive red dye used in the experiments.

Diafiltration experiments were then carried out at three different dye concentrations: 3.5 $mol \cdot m^{-3}$, 14 $mol \cdot m^{-3}$, and 35 $mol \cdot m^{-3}$. The initial salt concentration was 44 $mol \cdot m^{-3}$. In these experiments, a reservoir of 1 L capacity containing high purity water was inserted between the gas supply and the stirred cell. Permeate samples were taken every 15 to 20 mL and analyzed using the conductivity meter. The experiments were stopped when the chloride concentration in the feed solution (calculated using a mass balance analysis of the system) was reduced to about 5 $mol \cdot m^{-3}$. In all experiments involving dye solutions, the stirring speed was set at 400 rpm.

The chloride concentration in the dye solutions was measured using a chloride ion selective electrode. In pure salt solutions and the permeate solutions, the concentration was determined from conductivity measurements. For both methods, standards were prepared at different concentrations and the measured values were obtained using the calibration curves. Rejections reported for simple solutions of salts and solutes are accurate to within 1% and rejections for dye solutions are accurate to within 5%.

Results and Discussion

Characterization of the dye solute

Since the dye has three strong acidic functional groups, it is expected to behave as a strong electrolyte. Thus, theoretically, it is possible to estimate the limiting diffusivity of the dye from its limiting conductance, which can be obtained from the measurement of the conductivity of dye solutions at different concentrations. Once the diffusion coefficient ($D_{dye,\infty}$) is known, the solute radius (r_s) (m) can be determined using

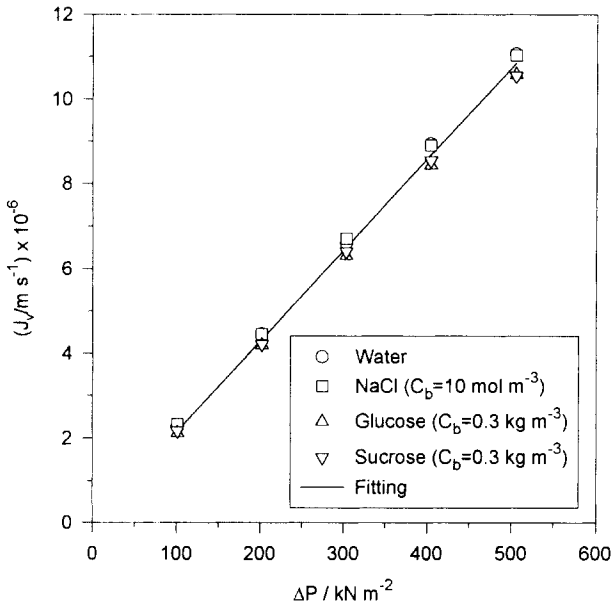

Figure 3. Fluxes vs. pressure drop for pure water, salts, and uncharged solutes.

the Stokes-Einstein equation (see Appendix). The diffusion coefficient at infinite dilution for the dye ion was determined to be 0.36×10^{-9} $m^2\cdot s^{-1}$. From this, the effective spherical radius of the dye was calculated as 0.63 nm.

Characterization of membrane

The CA30 membrane was chosen for the experiments with the dye/salt system since the dye did not irreversibly adsorb on the membrane. Preliminary experiments with the CA30 membrane showed that the dye rejection was greater than 98% and that the membrane retained its initial condition without any significant reduction in pure water permeability after washing with water.

Based on the previous findings with the NF-PES5 membrane (Bowen et al., 1997), the CA30 membrane was characterized using uncharged solutes to obtain r_p and $\Delta x/A_k$, and using salts (NaCl, KCl, LiCl) to obtain the effective charge density X_d. In addition further experiments with NaCl at different concentrations were carried out in order to obtain the variation of X_d with Cl^- concentration.

Figure 3 shows plots of solvent flux vs. pressure drop for various solutes and salt solutions compared to the pure water flux. The fluxes were close to that of pure water, showing that the osmotic pressure of the solutions was small. Figure 4 shows plots of real rejection (R_{real}) vs. fluxes for uncharged solutes. The data were fitted to obtain r_p and $\Delta x/A_k$ independently. Table 2 shows the results of the fitting for the uncharged solutes.

Table 2. Result of Fitting for Uncharged Solutes

Solutes	λ	$\Delta x/A_k$ (μm)	r_p (nm)
Glycerin	0.418	2.65	0.62
Glucose	0.595	1.92	0.61
Sucrose	0.714	0.74	0.66
Vitamin B_{12}	0.853	0.39	0.87

The average pore size using all four solutes was 0.69 nm. The average pore size obtained using glycerin, glucose and sucrose was 0.63 nm and the values for each were close. Figure 5 shows that the limiting rejection of the solutes R_{lim} were well fitted using $r_p = 0.63$ nm. Therefore, for subsequent work, this value will be used as the effective pore radius of the membrane. As was observed with the NF-PES5 membrane (Bowen et al., 1997), the value of $\Delta x/A_k$ de-

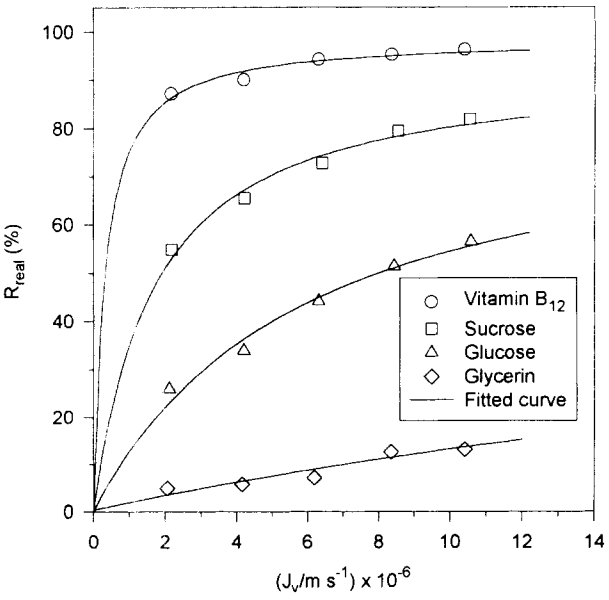

Figure 4. Rejection of various uncharged solutes as a function of flux.

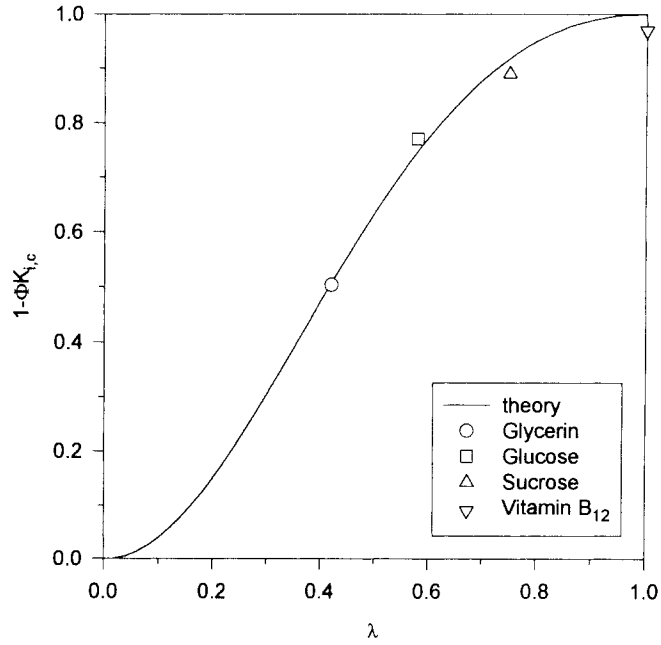

Figure 5. Limiting rejection of solutes as a function of $\lambda = r_s/r_p$.

Data were assessed for $r_p = 0.63$ nm.

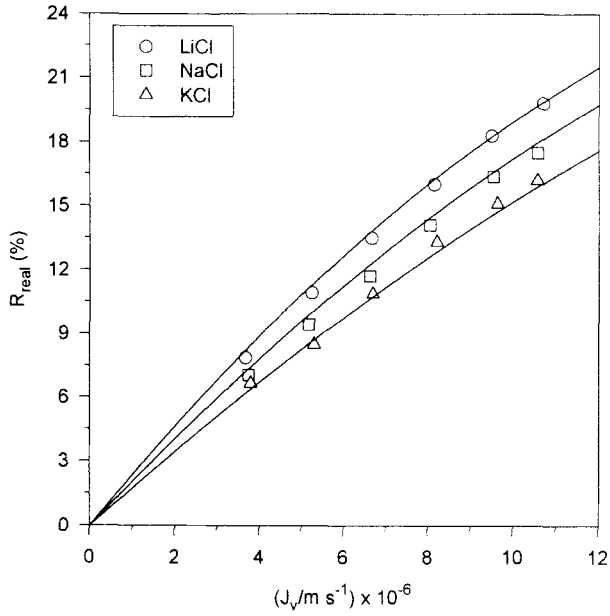

Figure 6. Rejection of KCl, NaCl, and LiCl at $C_b = 10$ mol·m^{-3}.

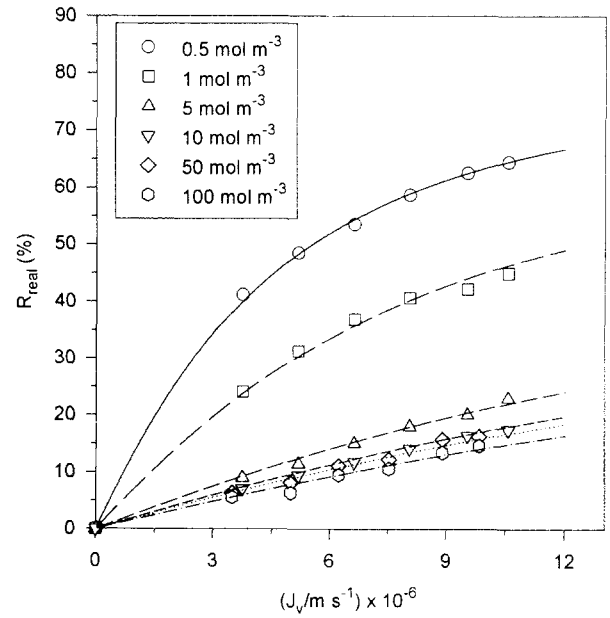

Figure 7. Rejection of NaCl at different ionic strengths.

creases as the solute radius increases. This indicates that larger solutes have shorter transport paths due to their inability to enter the smaller of the network pores in the membrane. The pore radius obtained using data for vitamin B_{12} was significantly greater than that obtained using the other solutes. As shown in Figure 4, the rejection of vitamin B_{12} was high (> 90%) and did not vary greatly with J_v. This makes it more difficult to estimate r_p from the data. Transmission of vitamin B_{12} may in practice be occurring through a few large pores in the membrane.

Figure 6 shows plots of R_{real} vs. J_v for the three salts at $C_b = 10$ mol·m^{-3}. The data were fitted using the extended Nernst-Planck equations assuming a porous membrane, that is, the Donnan-steric-pore (DSPM) model. The plot shows that the rejection sequence follows LiCl > NaCl > KCl which is the reverse of that obtained using NF-PES5 (Bowen et al., 1997). This suggests that in the present case the steric effect is significant at the entrance of membrane. The fitting of the data confirmed that a good fit was only possible by inclusion of the steric partitioning term in the equilibrium conditions at the entrance of the pores. The fittings shown were carried out by assuming that $r_p = 0.63$ nm as obtained using uncharged solutes. Table 3 shows the result of the fittings.

Figure 7 shows R_{real} vs. J_v for NaCl at different concentrations. The fitted lines were those obtained using the DSPM model. In these fittings, r_p and $\Delta x/A_k$ were fixed at 0.63 nm and 6.2 μm, respectively, and only X_d was fitted. Figure 8 shows the variation of $|X_d|$ as a function of concentration. As obtained previously for NF-PES5 (Bowen and Mukhtar, 1995), $|X_d|$ increases as concentration increases. Similar behavior has been reported for different types of membranes (Aitkuliev et al., 1984; Tsuru et al., 1991b; Wang et al., 1995). In the present case, the variation of $|X_d|$ with C_b was linear.

Table 3. Result of Fitting Obtained Using Salts

Salts	C_b (mol·m^{-3})	$-X_d$ (mol·m^{-3})	$\Delta x/A_k$ (μm)	S_y
NaCl, KCl, and LiCl	10.0	39.2	6.2	0.309
NaCl	0.5	10.7	$\Delta x/A_k$	0.683
	1.0	11.4	was fixed	1.262
	5.0	23.6	at 6.2 μm	0.634
	50.0	184.1		0.657
	100.0	333.6		0.785

$$*S_y = \left(\frac{\sum_{i=1}^{n} [R_{exp} - R_{calc}]^2}{n-1} \right)^{0.5}, \quad n = \text{number of observations}$$

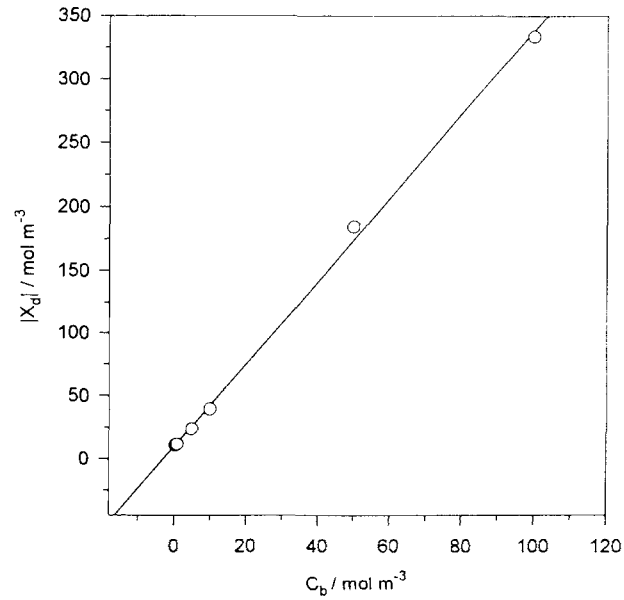

Figure 8. Charge density $|X_d|$ as a function of ionic strength.

The charge density can be related to the following linear isotherm

$$|X_d| = 9.03 + 3.29C_b \tag{38}$$

The quality of the agreement of fitted values of X_d to the experimental data is shown through the parameter S_y in Table 3.

Experiments at different dye/salt ratios

Figure 9 shows the flux of the dye solutions as a function of chloride concentrations in the solution. The fluxes were generally lower than water flux. The higher the dye concentration, the lower the flux of the dye solution. The flux behavior also seemed to be slightly influenced by the salt concentrations in the solutions. For $C_{\text{dye},b} = 37$ mol·m^{-3}, the flux increased as [Cl$^-$] increased but a reverse pattern was observed for $C_{\text{dye},b} = 4$ mol·m^{-3}.

Additional experiments were carried out at different stirring speeds. Figure 10 shows the permeate flux as a function of the stirring speed for $C_{\text{dye},b} = 37$ mol·m^{-3} and $C_{\text{salt},b} = 87$ mol·m^{-3}. The plot shows that the permeate flux increased as the stirring speed increased, which indicated that the osmotic pressure arising from the concentration polarization effect is quite significant. This effect was confirmed by calculating the osmotic pressure difference across the membrane using the van't Hoff law (Rautenbach and Albrecht, 1989; Mulder, 1991)

$$\Delta\pi = RT(\Sigma C_{i,w} - \Sigma C_{i,p}) \tag{39}$$

where the summation signs indicate that all components, both ions and dye, should be included.

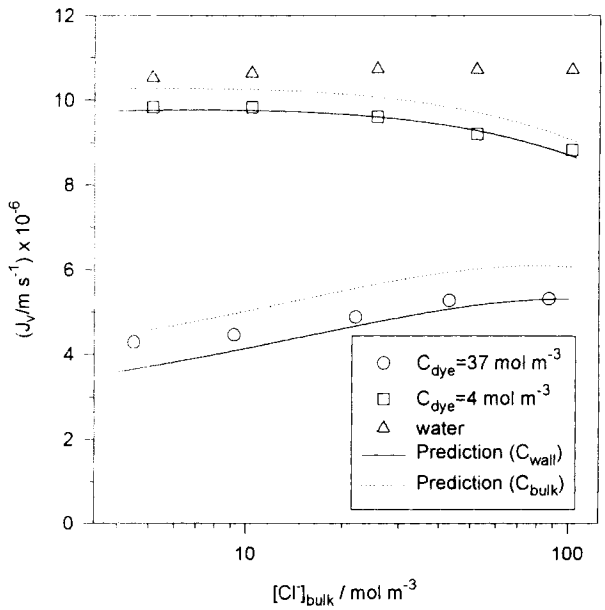

Figure 9. Permeate fluxes at different dye and Cl$^-$ concentrations.

Solid lines and dashed lines are predictions after correction using van't Hoff law.

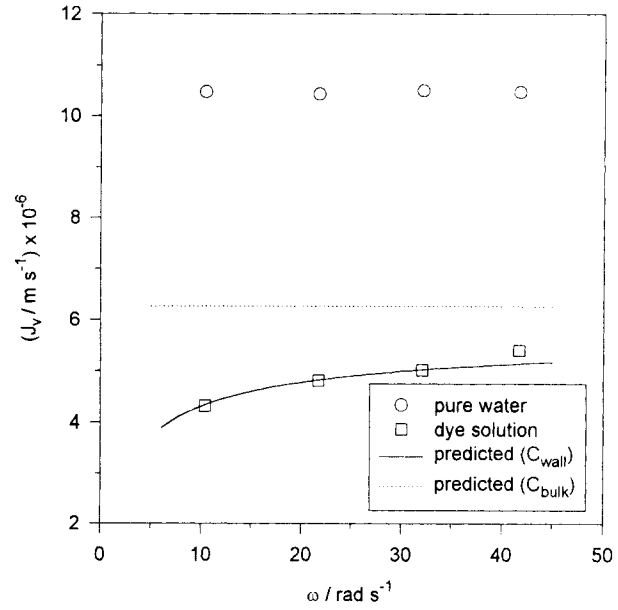

Figure 10. Permeate flux as a function of stirring speed.

$C_{b,\text{dye}} = 37$ mol·m^{-3}; $C_{b,\text{salt}} = 87$ mol·m^{-3}.

Thus, the permeate flux should be corrected as follows

$$J_v = \frac{r_p^2}{8\mu(\Delta x/A_k)}(\Delta P - \Delta\pi) \tag{40}$$

The solid lines and the dotted lines in Figures 9 and 10 show the calculated fluxes after allowing for the osmotic pressure based on the wall and bulk concentrations of the solutions, respectively. These concentrations were obtained through an iterative procedure using the model for transport through the membrane in conjunction with Eqs. 17 and 40. The figures show that in the presence of dye, the osmotic pressure can be significant and that this effect, and also the variation with salt concentration and stirring speed, were well quantified using the proposed concentration polarization model.

Figure 11 shows the observed rejection R_{obs} vs. feed chloride concentration for two concentrations of dye. Instead of using the real rejection R_{real}, R_{obs} is used in all the experiments with dye since R_{obs} represents a parameter that can be directly experimentally determined. Based on the dye and membrane characterization described previously, the dye is expected to be completely rejected sterically. However, the experimental data show that the rejection of the dye was 98–99%. This was probably due to the existence of a few larger pores in the membrane due to the pore-size distribution.

The solid lines in the plot were the predicted rejections for Na^+ and Cl^- based on the parameters (r_p, $\Delta x/A_k$, and X_d) obtained from the characterization of the membrane using salts and uncharged solutes. The predictions, however, were found to be good only when the charge density X_d was taken to be a function of the total concentration of anions in the feed solution $C_{T,-ve}$ (mol·m^{-3}) which was equivalent to the concentration of Na^+ ions

$$C_{T,-ve} = C_{Na^+} = 3C_{\text{dye},b} + C_{Cl^-,b} \tag{41}$$

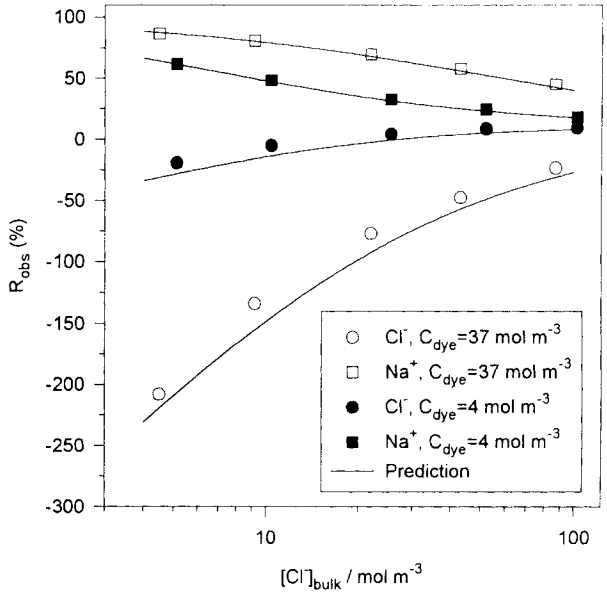

Figure 11. Rejections of ions at different ratios of dye/ Cl^- solutions.

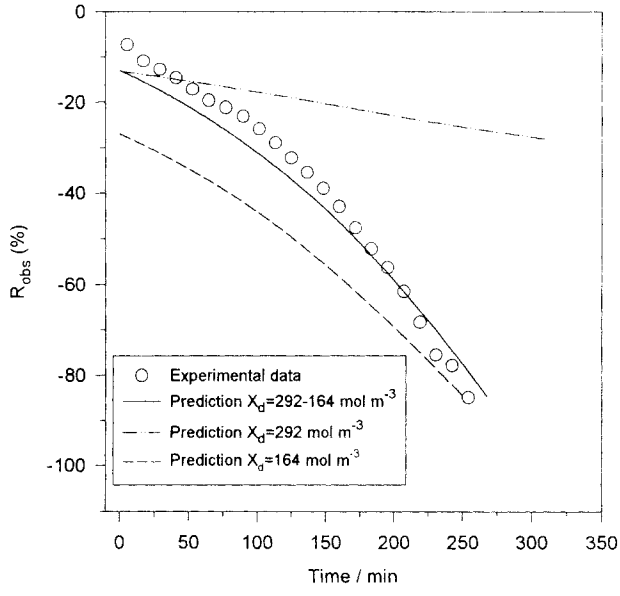

Figure 12. Prediction of rejection using fixed and varied X_d for $C_{b,\ dye}=14$ mol·m^{-3}.

The fact that the prediction worked only when X_d is correlated to $C_{T,-ve}$ was quite surprising. Previous findings (Bowen and Mukhtar, 1996) for the ternary salt system (Na^+:Cl^-:SO_4^{2-}) showed that X_d can be correlated well to an isotherm based on the total equivalent concentration of co-ions in the solutions. For the work with dye, it might be thought that, since the dye was almost completely rejected, the dye concentration would have no effect on X_d of the membrane. However, the higher the dye concentration while maintaining the same concentration of Cl^- in the feed, the more Cl^- will permeate through the membrane and if co-ion adsorption takes place, it would be expected that X_d then will be higher. Thus, the dye concentration is indirectly affecting the charge density inside the membrane. Equation 41 is based on bulk concentrations rather than wall concentrations. This simplification is made for two reasons. First, the magnitude of concentration polarization is not great. Secondly, and more importantly, expressing Eq. 41 in terms of membrane wall concentrations would give values of X_d which depended on the membrane flux, considerably complicating the theoretical analysis.

The predictions shown in Figure 11 were made by assuming that the dye ion was completely rejected by the membrane. That is, only the transport of Na^+ and Cl^- ions is taken into account inside the membrane. Concentration polarization was taken into account using the method described earlier. The thickness of the film layer δ was taken as 24.3 μm, determined from the mass-transfer coefficient of the dye based on the determined diffusion coefficient as described in the fourth section. The agreement between the predictions and the experimental data is very good.

Diafiltration experiments

The diafiltration experiments were carried out at three different dye concentrations: 3.5 mol·m^{-3}, 14 mol·m^{-3}, and 35 mol·m^{-3}. The initial salt concentration in the solution was 44 mol·m^{-3}. The experiments were continued until the salt concentration in the solutions reached about 5–6 mol·m^{-3}, based on a mass balance analysis for the system. During the diafiltration experiments, the variation of fluxes at different dye concentrations as a function of salt concentrations in the feed solutions follows the pattern obtained in the experiments at different dye/salt ratios as described in the previous section.

Figure 12 shows the rejection of Cl^- as a function of time for $C_{dye,b}=14$ mol·m^{-3}. Three different predictions were made. The first and second predictions assumed that X_d corresponded to the maximum and minimum $C_{T,-ve}$, respectively. The third prediction assumed that X_d varied as a function of $C_{T,-ve}$, as defined in Eq. 40. The plot clearly shows that the best prediction is that allowing for variation in X_d as the salt concentration in the solution changed as a function of time.

Figure 13 shows the overall results for the rejection of Cl^- and Na^+ at different dye concentrations. The results show that the predictions using r_p and $\Delta x/A_k$ obtained as described previously, and allowing for X_d to vary as a function of the total concentrations of negative charge in the system, are very good.

Perspective on Optimization

The purpose of any optimization is to obtain the most economically viable processing conditions. For a diafiltration process, the treatment time and the membrane area are the two key economic factors (Dutre and Tragardh, 1994). In this section two types of optimization will be discussed. The first is concerned with the optimization of the total processing time for the overall process, which includes pre- and post-concentration phases. The second seeks to find the optimum membrane characteristics for the diafiltration process. The main purpose is to show that the structural-based model as used here is useful not only in predicting the process per-

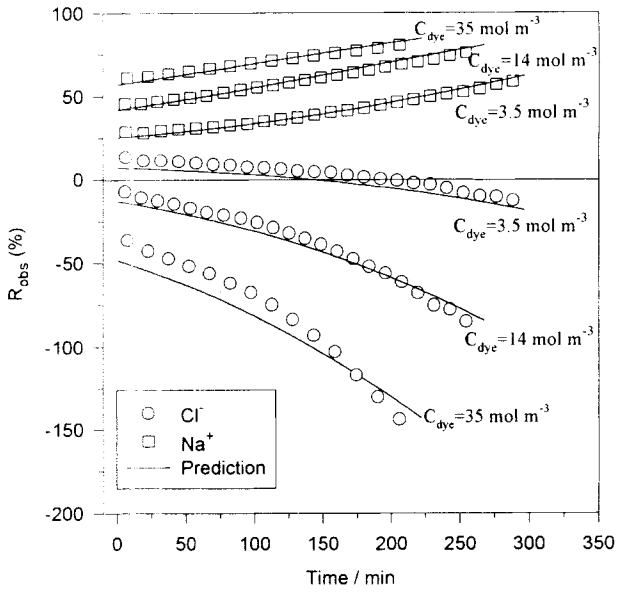

Figure 13. Prediction of rejection of salts during diafiltration at different dye concentrations.

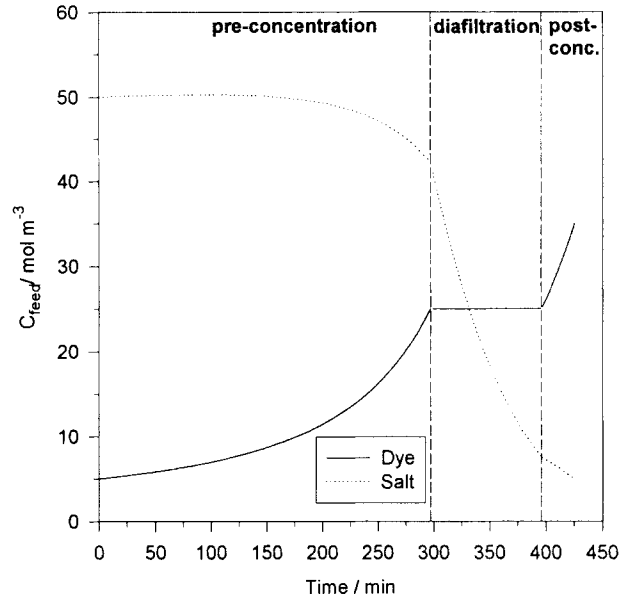

Figure 14. Concentration variation during the three phases.

formance, but also in optimizing the processing conditions and the membrane parameters.

Optimizing the overall processing time

The optimization of the processing time must include the period for pre- and post-concentration of the treated solutions (Ali Asbi and Cheryan, 1992; Jaffrin and Charrier, 1994). In this work, the overall process will be optimized in order to find the mode of operation that will give the shortest processing time.

In order to carry out such optimization, the behavior of permeate flux at different dye and salt concentrations must be known. The experimental results show that the permeate flux can be determined by taking into account the osmotic pressure difference using the van't Hoff equation. The wall concentration may be determined using the concentration polarization model. The optimization of the overall process was carried out in terms of a normalized processing time which was defined as the time needed to process 1 mol of dye using 1 m^2 of membrane area. The initial solution was assumed to contain 5 mol·m^{-3} of dye and 50 mol·m^{-3} of salt. It is intended to reduce the salt concentration to 5 mol·m^{-3} and to increase the dye concentration to 35 mol·m^{-3}.

The calculation was carried out for seven different cases depending on the intended target for C_{dye} in the preconcentration phase. The targeted C_{dye} in the preconcentration phases was varied from 35 mol·m^{-3} to 5 mol·m^{-3}. Then, diafiltration and post-concentration will be carried out to obtain the final dye and salt concentrations. For case 1, no post-concentration phase is needed, while for case 7, no preconcentration phase is needed.

Figure 14 shows an example of the variation in the concentrations of dye and salt during the three phases. The salt concentration is always changing during all the phases while the dye concentration varies according to the set criteria. Table 4 shows the results of the calculations. The results show that case 1, where no post-concentration is needed, gives the shortest overall processing time. In this case, the concentration of dye is maximum while the treated volume is minimum during the diafiltration phase. A similar conclusion was observed in the case of diafiltration of human albumin using ultrafiltration membranes (Jaffrin and Charrier, 1994). Thus, it can be concluded that, unless there is some other mechanism of flux reduction, the shortest processing time will be obtained by operating at the maximum dye concentration during the diafiltration phase for the dye concentration range studied. However, at higher dye concentrations, other flux reduction mechanisms may become important (for example,

Table 4. Results for Optimization Study

	Init. Conditions		Preconcentration			Diafiltration		Post-Concentration			Total Time
Case	$C_{dye,0}$ (mol·m^{-3})	$C_{salt,0}$ (mol·m^{-3})	$C_{dye,1}$ (mol·m^{-3})	$C_{salt,1}$ (mol·m^{-3})	Time (t_1) (min)	$C_{salt,2}$ (mol·m^{-3})	Time (t_2) (min)	$C_{dye,3}$ (mol·m^{-3})	$C_{salt,3}$ (mol·m^{-3})	Time (t_3) (min)	($t_1+t_2+t_3$) (min)
1	5	50	35	35.1	350.6	5	95.8	35	—	—	446.4
2	5	50	30	38.3	334.7	6.4	98.3	35	5.0	18.5	451.3
3	5	50	25	41.5	315.3	7.9	106.3	35	5.0	39.7	461.3
4	5	50	20	44.6	289.8	9.8	119.8	35	5.0	66.4	476.0
5	5	50	15	47.4	252.0	11.8	146.7	35	5.0	104.9	503.6
6	5	50	10	49.6	184.1	14.1	203.1	35	5.0	172.2	559.4
7	5	50	5	50.0	—	16.2	380.7	35	5.0	353.8	734.5

deposition of the dye on the membrane) and the shortest processing time may then be achieved at a dye concentration below the maximum.

Optimizing the membrane parameters

In this work, the membrane was characterized in terms of the pore radius r_p (m), effective thickness over porosity $\Delta x/A_k$, and the membrane charge density X_d. The r_p was determined to be 0.63 nm. It was observed experimentally that for a dye of similar size ($r_s = 0.63$ nm), the rejection was 98–99%. If the membrane had lower r_p, the dye is expected to be completely rejected. However, reducing r_p would result in a reduction of flux (for a given applied pressure) unless there was a compensating change in $\Delta x/A_k$.

Reducing r_p would also result in less negative rejection of Cl^- due to steric partitioning, which would reduce the efficiency of the diafiltration process. Thus, a more effective strategy to achieve a higher dye rejection might be to choose a membrane with a more negative X_d. In general, all three membrane parameters, as well as the operating pressure and solution mass transfer, influence the separation achieved. However, the approach described in this article allows identification of the membrane parameters which will give a desired separation. The membrane which most closely matches these requirements may then be selected.

Conclusions

A diafiltration process involving a mixture of dye and NaCl has been modeled using a Donnan-steric pore model which was based on the extended Nernst-Planck equation. The membrane (CA30) was characterized in terms of an effective pore radius (r_p), effective thickness over porosity ($\Delta x/A_k$), and effective charge density (X_d) using rejection data of uncharged solutes and binary salt solutions.

Individual experiments at different dye/salt ratios were carried out at constant pressure. The rejections of Cl^- and Na^+ were predicted in terms of r_p, $\Delta x/A_k$, and X_d using the model. It was found that an excellent prediction was obtained if it was assumed that X_d was dependent on the total concentration of negative charges in the solutions. A description of concentration polarization in mixtures of charged species was also included in the model. For our experimental conditions, it was determined that the concentration polarization effect was small.

Diafiltration experiments were carried out at three different dye concentrations. In each the salt concentration was reduced from 44 mol·m^{-3} to about 6 mol·m^{-3}. The prediction of the process performance was excellent. Finally, the model was used to investigate optimization of the processing conditions and also the membrane parameters. Based on normalized processing time, the overall diafiltration process was found to be best operated in a two-phase mode where the dye solution is preconcentrated to the final dye concentration before diafiltration is carried out.

Acknowledgment

This article forms part of a work program funded by the UK BBSRC. The Universiti Kebangsaan Malaysia is thanked for providing support to A. Wahab Mohammad. Dr Kumar Abhinava from Zeneca is thanked for useful discussion and for providing the dye sample.

Notation

A = total membrane area, m^2
A_k = effective porosity of the membrane
$C_{i,b}$ = concentration in the bulk solution, mol·m^{-3}
C_T = total concentration in solution, mol·m^{-3}
$D_{i,p}$ = hindered diffusivity, m^2·s^{-1}
$D_{i,\infty}$ = bulk diffusivity, m^2·s^{-1}
F = Faraday constant, C·mol^{-1}
I_c = current density, A·m^{-2}
J_v = volume flux (based on membrane area), m·s^{-1}
J_w = water flux (based on membrane area), m·s^{-1}
k_B = Boltzmann's constant
M_{dye} = mass of dye in feed solution, kg
ΔP = applied pressure drop, kN·m^{-2}
r = radius of stirrer, m
R = gas constant, J·mol^{-1}·K^{-1}
S_v = standard deviation of the experimental data
t_c = time during concentration phase, s
t_d = time during diafiltration phase, s
T = absolute temperature, K
T_1 = total time for diafiltration, s
u_i = mobility of ion, m^2·s^{-1}·V^{-1}
V = solute velocity, m·s^{-1}
V_f = feed volume during diafiltration, m^3
x = distance normal to membrane, m
$\Delta\pi$ = osmotic pressure difference, kN·m^{-2}
z_i = valence of ion
γ_i^0 = activity coefficient for ion i in the bulk solution
γ_i = activity coefficient for ion i inside the membrane pores
μ = viscosity of solution, Pa·s
ν = kinematic viscosity, m^2·s^{-1}
ω = stirring speed, s^{-1}
ψ_m = electric potential in axial direction inside membrane, V
ψ_f = electric potential in axial direction in film layer, V
$\Delta\psi$ = potential difference in solution, V
$\Delta\psi_D$ = Donnan potential difference, V

Subscripts

c_0 = initial value during concentration phase
c_1 = final value during concentration phase
d_0 = initial value during diafiltration phase
d_1 = final value during diafiltration phase
dye f = dye in feed solution
sf = salt in feed solution
sp = salt in permeate solution
∞ = bulk property

Literature Cited

Aitkuliev, K., V. D. Sobolev, and N. V. Churaev, "Influence of the Flow Rate and Concentration of the Electrolyte on the Selectivity of Reverse Osmosis Membranes," *Colloid J.*, **46**, 179 (1984).

Ali Asbi, B., and M. Cheryan, "Optimizing Process Time for Ultrafiltration and Diafiltration," *Desalination*, **86**, 49 (1992).

Atkins, P. W., *Physical Chemistry*, 4th ed., Oxford Univ. Press, Oxford (1990).

Boehringer Mannheim, Biochemicals Catalogue, Lewes (1996).

Bowen, W. R., and A. O. Sharif, "Transport Through Microfiltration Membranes: Particle Hydrodynamics and Flux Reduction," *J. Colloid Interf. Sci.*, **168**, 414 (1994).

Bowen, W. R., and H. Mukhtar, "Characterisation and Prediction of Separation Performance of Nanofiltration Membranes," *J. Memb. Sci.*, **112**, 263 (1996).

Bowen, W. R., A. W. Mohammad, and N. Hilal, "Characterisation of Nanofiltration Membranes for Predictive Purposes—Use of Salts, Uncharged Solutes and Atomic Force Microscopy," *J. Memb. Sci.*, **126**, 91 (1997).

Burghoff, H. G., K. L. Lee, and W. Pusch, "Characterization of Transport Across Cellulose-Acetate Membranes in the Presence of Strong Solute-Membrane Interactions," *J. Applied Poly. Sci.*, **25**, 323 (1980).

Crow, D. R., *Principles and Applications of Electrochemistry*, 4th ed., Blackie Academic & Professional, Glasgow (1994).

Cussler, E. L., *Diffusion: Mass Transfer in Fluid Systems*, Cambridge University Press, U.K. (1995).
Deen, W. M., B. Satvat, and M. Jamieson, "Theoretical Model for Glomerular Filtration of Charged Solutes," *Amer. J. of Physiology*, **38**, 126 (1980).
Deen, W. M., "Hindered Transport of Large Molecules in Liquid-Filled Pores," *AIChE J.*, **33**, 1409 (1987).
Dickson, J. M., "Fundamental Aspects of Reverse Osmosis," *Reverse Osmosis Technology: Application for High-Purity-Water Production*, B. S. Parekh, ed., Marcel Dekker, New York, p. 1 (1988).
Dutre, B., and G. Tragardh, "Macrosolute-Microsolute Separation by Ultrafiltration: A Review of Diafiltration Processes and Applications," *Desalination*, **95**, 227 (1994).
Helfferich, F., "Ion-Exchange Kinetics—Evolution of a Theory," *Mass Transfer and Kinetics of Ion Exchange*, NATO Advanced Study Institute Series E: Applied Sciences, No. 71, L. Liberti and F. G. Helfferich, eds., Martinus Nijhoff, The Hague (1983).
Jaffrin, M. Y., and J. Ph. Charrier, "Optimization of Ultrafiltration Processes for Albumin Production," *J. Memb. Sci.*, **97**, 71 (1994).
Jitsuhara, I., and S. Kimura, "Rejection of Inorganic Salts by Charged Ultrafiltration Membranes Made of Sulfonated Polysulfone," *J. Chem. Eng. Japan*, **16**, 394 (1983).
Krishna, R., and J. A. Wesselingh, "The Maxwell-Stefan Approach to Mass Transfer," *Chem. Eng. Sci.*, **52**(6), 861 (1997).
Levenstein, R., D. Hasson, and R. Semiat, "Utilisation of the Donnan Effect for Improving Electrolyte Separation with Nanofiltration Membranes," *J. Memb. Sci.*, **116**, 77 (1996).
Mulder, M., *Basic Principles of Membrane Technology*, Kluwer, Dordrecht, The Netherlands (1991).
Nakao, S., and S. Kimura, "Analysis of Solutes Rejection in Ultrafiltration," *J. Chem. Eng. Japan*, **14**, 32 (1981).
Opong, W. S., and A. L. Zydney, "Diffusive and Convective Protein Transport Through Asymmetric Membranes," *AIChE J.*, **37**, 1497 (1991).
Perry, M., and C. Linder, "Intermediate RO UF Membranes for Concentrating and Desalting of Low Molecular Weight Organic Solutes," *Desalination*, **71**, 233 (1989).
Raman, L. P., M. Cheryan, and N. Rajagopalan, "Consider Nanofiltration for Membrane Separations," *Chem. Eng. Prog.*, **90**, 68 (1994).
Rautenbach, R., and R. Albrecht, *Membrane Processes*, Wiley, Chichester, U.K. (1989).
Rios, G. M., R. Joulie, S. J. Sarrade, and M. Carles, "Investigation of Ion Separation by Microporous Nanofiltration Membranes," *AIChE J.*, **42**(9), 2521 (1996).
Sato, H., M. Yui, and H. Yoshikawa, "Ionic Diffusion Coefficient of Cs^-, Pb^{2+}, Sm^{3+}, Ni^{2+}, SeO_4^{2-}, and TcO_4^- in Free Water Determined from Conductivity Measurements," *J. Nucl. Sci. and Tech.*, **33**(12), 950 (1996).
Schirg, P., and F. Widmer, "Characterisation of Nanofiltration Membranes for the Separation of Aqueous Dye-Salt Solutions," *Desalination*, **89**, 89 (1992).
Smith, K. A., C. K. Colton, E. W. Merrill, and L. B. Evans, "Convective Transport in a Batch Dialyzer: Determination of True Membrane Permeability from a Single Measurement," *AIChE Symp. Ser.*, **64**, 45 (1968).
Spiegler, K. S., and O. Kedem, "Thermodynamics of Hyperfiltration (RO): Criteria for Efficient Membranes," *Desalination*, **1**, 311 (1966).
Tawarah, K. M., and A. A. Wazwaz, "The Electrical Conductivities of the Sodium Salts of Methyl Orange, 0-Methyl Red and p-Methyl Red in Aqueous Solutions," *Dyes and Pigments*, **21**, 97 (1993).
Tsuru, T., S. Nakao, and S. Kimura, "Calculation of Ion Rejection by Extended Nernst-Planck Equation with Charged Reverse Osmosis Membranes for Single and Mixed Electrolyte Solutions," *J. Chem. Eng. Japan*, **24**, 511 (1991a).
Tsuru, T., M. Urairi, S. Nakao, and S. Kimura, "Reverse Osmosis of Single and Mixed Electrolytes with Charged Membranes: Experiment and Analysis," *J. Chem. Eng. Japan*, **24**, 518 (1991b).
van der Wielen, L. A. M., M. Zomerdijk, J. Houwers, and K. Ch. A. M. Luyben, "Diffusivities of Organic Electrolytes in Water," *Chem. Eng. J.*, **66**, 111 (1997).
Wang, X. L., T. Tsuru, M. Togoh, S. Nakao, and S. Kimura, "Evaluation of Pore Structure and Electrical Properties of Nanofiltration Membranes," *J. Chem. Eng. Japan*, **28**, 186 (1995a).
Wang, X. L., T. Tsuru, M. Togoh, S. Nakao, and S. Kimura, "Transport of Organic Electrolytes with Electrostatic and Steric-Hindrance Effects Through Nanofiltration Membranes," *J. Chem. Eng. Japan*, **28**, 372 (1995b).
Wesselingh, J. A., and P. Vonk, "Ultrafiltration of a Large Polyelectrolyte," *J. Memb. Sci.*, **99**, 21 (1995).

Appendix

Theory for limiting conductance of strong electrolytes

Conductivity measurement can provide an accurate determination of diffusion coefficient of ionic species in an aqueous system (Cussler, 1995). It has been used quite successfully for various inorganic ions (Sato et al., 1996), dyes (Tawarah and Wazwaz, 1993) and various large organic ions (van der Wielen et al., 1997) in aqueous solutions. This section describes briefly the theory and results of the measurement of conductivity to determine the infinite diffusivity value for the dye ion that was used in the present study.

For strong electrolyte solutions, the electrical conductivity which is the reciprocal of the electrical resistance of the solution can be measured easily using a conductivity meter. The resistance is inversely proportional to the current flowing between the two electrodes. It can be shown that the equivalent conductance Λ ($\Omega^{-1}\cdot cm^2\cdot mol^{-1}$), which is the most convenient measure of conductivity, is given by (Cussler, 1995)

$$\Lambda = |z_1|u_1 + |z_2|u_2 = \{(R)[K_{cell}F\nabla\psi]|z_1 z_2|c_T\}^{-1} \quad \text{(A1)}$$

The mobility of each ion in the above equation can be related to the diffusion coefficient $D_{i,\infty}$ ($m^2\cdot s^{-1}$)

$$D_{i,\infty} = k_B T u_i = \left[\frac{k_B T}{|z_i|}\right]\lambda_i \quad \text{(A2)}$$

where $\lambda_i = |z_i|u_i$ ($\Omega^{-1}\cdot cm^2\cdot mol^{-1}$) is defined as the equivalent ionic conductance of the ion. Thus, if the equivalent conductance of a solution such as the dye solution which contains dye ions and Na^+ ions is known, it is possible to determine the diffusion coefficient of the dye from the measurement of equivalent conductance of the solution.

The equivalent conductance is known to vary with concentration as expressed by the following equation (Crow, 1994)

$$\Lambda = \Lambda_0 - (B_1\Lambda_0 + B_2)\sqrt{c_T} + B_3 c_T\left(1 - B_1\sqrt{c_T}\right) \quad \text{(A3)}$$

where all B_i are constants. The limiting conductance Λ_0 is a property of the ions and is not well understood theoretically. This limiting value can be used to determine the infinite dilution diffusion coefficient of the ions. The constant of the second term in the equation is a function only of the charges on the ions and is thus characteristic of the electrostatic interactions between the ions. The constants in subsequent terms include other interactions such as ion-solute interactions and the ion associations more commonly encountered with weak electrolytes.

In this work, the conductance of the dye solutions was measured at different concentrations. The data were fitted to Eq. A3 from which the limiting ionic conductance was determined. Since the infinite dilution diffusion coefficient of Na^+

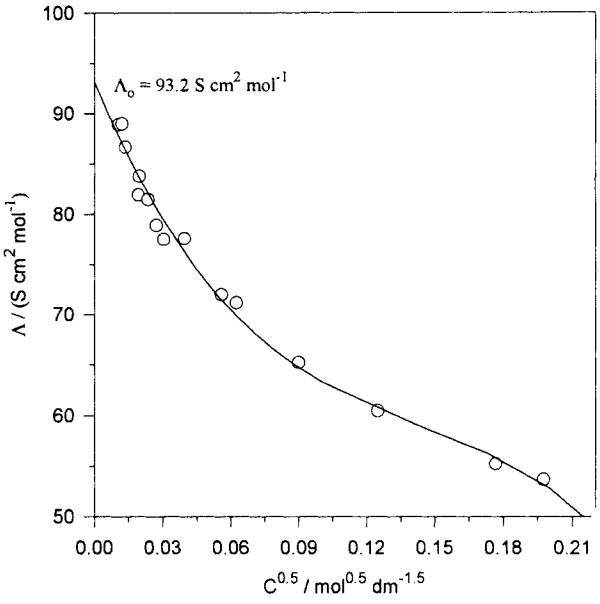

Figure A1. Equivalent conductances of dye solutions as function of concentration.

is known, the diffusion coefficient of the dye ion can be calculated from Eqs. A1 and A2. This will give the value of $D_{\infty,\text{dye}}$ at infinite dilution. The effective spherical radius of the dye ion can be determined from the Stokes-Einstein relation

$$r_{s,\text{dye}} = \frac{k_B T}{6\pi\mu D_{\text{dye},\infty}} \tag{A4}$$

Figure A1 shows the plot of the equivalent conductances vs. square root of the concentrations. The data were fitted well with Eq. A3. The limiting equivalent conductance for the dye was determined to be 93.1 $\text{cm}^2\cdot\Omega^{-1}\cdot\text{mol}^{-1}$. Equations A2 and A3 can be combined to give

$$\Lambda_0 k_B T = |z_1| D_{1,\infty} + |z_2| D_{2,\infty} \tag{A5}$$

Based on the literature value for $D_{\text{Na}^+,\infty}$, the diffusion coefficient for the dye^{3-} was found to be 0.36×10^{-9} $\text{m}^2\cdot\text{s}^{-1}$. Then, using Eq. A4, the effective spherical radius of the dye ion was calculated to be 0.63 nm.

Manuscript received Oct. 15, 1997, and revision received May 13, 1998.